Energy efficient F atom generation and control in CF$_4$ capacitively coupled plasmas driven by tailored voltage waveforms

Xiao-Kun Wang[1,2] ![ORCID], Ranna Masheyeva[3,4] ![ORCID], Yong-Xin Liu[1,*] ![ORCID], Yuan-Hong Song[1] ![ORCID], Peter Hartmann[3] ![ORCID], Zoltán Donkó[3] ![ORCID] and Julian Schulze[2] ![ORCID]

[1] Key Laboratory of Materials Modification by Laser, Ion, and Electron Beams (Ministry of Education), School of Physics, Dalian University of Technology, Dalian 116024, People's Republic of China
[2] Chair of Applied Electrodynamics and Plasma Technology, Department of Electrical Engineering and Information Sciences, Ruhr-University Bochum, D-44780 Bochum, Germany
[3] Institute for Solid State Physics and Optics, HUN-REN Wigner Research Centre for Physics, 1121 Budapest, Hungary
[4] Department of General Physics, Satbayev University, 050013 Almaty, Kazakhstan

E-mail: yxliu129@dlut.edu.cn

CrossMark

Abstract

Neutral radicals generated by electron impact dissociation of the background gas play important roles in etching and deposition processes in low pressure capacitively coupled plasmas (CCPs). The rate and energy efficiency of producing a given radical depend on the space- and time-dependent electron energy distribution function (EEDF) in the plasma, as well as the electron energy dependent cross sections of the electron-neutral collisions that result in the generation of the radical. For the case of a CCP operated in CF$_4$ gas, we computationally demonstrate that the energy efficiency of generating neutral radicals, such as F atoms can be improved by controlling the EEDF by using tailored voltage waveforms (TVW) instead of single-frequency driving voltage waveforms and that separate control of the radical density and the ion energy can be realized by adjusting the waveform shape at constant peak-to-peak voltage. Such discharges are often used for industrial etching processes, in which the F atom density plays a crucial role for the etch rate. Different voltage waveform shapes, i.e. sinusoidal waveforms at low (13.56 MHz) and high (67.8 MHz) frequencies, peaks- and sawtooth-up TVWs, are used to study their effects on the energy cost / energy efficiency of F atom generation by PIC/MCC simulations combined with a stationary diffusion model. The F atom density is enhanced by increasing the voltage amplitude in the single frequency cases, while the energy cost per F atom generation increases, i.e. the energy efficiency decreases, because more power is dissipated to the ions, as the sheath voltages and the ion energy increase simultaneously. In contrast, using TVWs can result in a lower energy cost and provide separate control of the F atom density and the ion energy. This is explained by the fact that tailoring the waveform shape in this way allows to enhance the high-energy tail of the EEDF during the sheath expansion phase by inducing a non-sinusoidal sheath motion, which results in acceleration of more electrons to high enough energies to generate F atoms via electron-neutral collisions

* Author to whom any correspondence should be addressed.

compared to the single frequency cases. Similar effects of TVWs are expected for the generation of other neutral radicals depending on the electron energy threshold and the specific consequences of TVWs on the EEDF under the discharge conditions of interest.

1. Introduction

Fluorine-containing gases are extensively used for etching silicon-based materials, such as silicon dioxide (SiO_2) and silicon nitride (Si_3N_4) in the fabrication of semiconductor devices, especially in radio frequency (RF) capacitively coupled plasmas (CCP). Often complex reactive gases and gas mixtures, characterized by complex plasma chemistries and plasma-surface interactions are used such as CF_4/H_2, CF_4/O_2, C_4F_8, CHF_3, and SF_6/O_2. In these applications, the F atoms produced in the discharge are the main etchant [1, 2]. For the development of plasma-etching techniques, the etch rates by which free radicals react with various substrates are important. Fluorine atoms are the principal gaseous reactant in many common etching processes. By exposing such wafer materials to F atom and ion fluxes, the silicon compounds react to form volatile silicon fluorides, which are easily removed from the surface, allowing for a controlled etching of these materials. However, achieving high etch selectivity still remains one of the main challenges in this field [1, 3]. For this purpose the separate control of the fluxes of reactive radicals and energetic ions to the wafer is essential. The etch mechanisms in fluorocarbon discharges have been studied thoroughly [4–6]. Enhancing the etch rate is very important for increasing the throughput. To achieve this, a comprehensive understanding of the behavior of F atoms and the control of their generation rate in fluorocarbon discharges is essential and an important topic of research in both academia and industry [7–10].

In experiments, several methods have been used to measure the F atom density. In [11], the F atom density was measured by gas-phase titration with Cl_2 in a 50 cm upstream, 14 MHz RF discharge in F_2. The authors have found that the etch rate of silicon is proportional to the F atom density determined by the discharge power. Optical emission spectroscopy is a very useful diagnostic method, the intensity of the atomic F emission can be used as a reliable indicator of the relative F atom density [12, 13]. In a capacitively coupled CF_4 plasma driven by 13.56 MHz at 100 W, the F atom density determined by the F atom emission was found to increase as a function of pressure within the range around 140 mTorr, but an increasing flow rate resulted in a decrease of the F atom density. Actinometry based on the reactions of F atoms was also used for the measurement of the density of F atoms in [14–16].

In a CF_4+O_2 plasma sustained in a parallel plate configuration driven by 13.56 MHz at around 40 mTorr, the F atom density was found to increase first with the addition of O_2, and then to decrease when the fraction of O_2 was larger than about 20% [13]. Another optical method is vacuum ultraviolet absorption spectroscopy (VUVAS) [15, 17], by using this

method the range of the F atom density was found to be in the order of 10^{11}–10^{13} cm^{-3}, and to increase with RF power in the range of 0.2–1.6 kW in an electron-cyclotron resonance CF_4 plasma [8]. The limitation of this method is that it only provides the spatially-averaged density along the path of the probe and with technical issues of short wavelength and radiation trapping [7, 18]. Appearance mass spectrometry (AMS) can also be used to measure the F atom density, but similarly to the actinometry method, the spatially-resolved distribution of the F atom density cannot be obtained [19, 20]. The F atom density can also be determined from the CF_2 loss rate based on measurements by laser-induced fluorescence (LIF) spectroscopy [21]. Based on this method, the volume averaged F atom density was determined at different RF powers for a CF_4 plasma at 200 mTorr, i.e. at relatively low pressure conditions where significant density gradients are not expected. However, the method is based on many assumptions, the measurement results have a significant error of up to 50%.

In low pressure CCPs, in order to control the ion energy and ion flux independently for the optimization of plasma processes, dual-frequency (DF) driving voltage waveforms were introduced to realize this control by adjusting the low and high frequency voltage amplitude, respectively [22, 23]. Due to the coupling effects between the frequencies, the applicability of DF CCPs is, however, limited [24–26]. An alternative concept to achieve such independent control of ion energy and flux is based on the electrical asymmetry effect, which utilizes the phase angle between two (or more) consecutive harmonics forming the driving voltage waveform [27–30]. The mean ion energy can be adjusted by changing the DC self-bias via phase control of the amplitude or slope asymmetry of the driving voltage waveform while the ion flux remains (nearly) constant. This method also exhibits some limitations when the plasma operates in different discharge modes [31, 32]. In recent years, the use of non-sinusoidal waveforms, also known as tailored voltage waveforms (TVWs), became widespread to control the ion energy and flux [33–35]. This includes sawtooth-type voltage waveforms, characterized by different rising and falling slopes. Plasmas excited by this waveform exhibit unique properties such as low ion energies at high ion fluxes at the wafer [36–38]. Driving CCPs by TVWs requires the use of advanced multi-frequency impedance matchings, which have been developed [39–41].

In [42], the ion energy distribution function (IEDF) was found to exhibit a bi-modal shape and the maximum of the ion energy was found to decrease at a constant ion flux at the electrodes as a function of the number of harmonics used to synthesize the TVW at a low pressure of 5 mTorr in a capacitively coupled Ar plasma driven by sawtooth waveforms.

Such conditions are preferable for heat sensitive materials in plasma processes. The findings of [43] suggest that a larger DC self-bias and higher ion energy can be generated at a lower driving frequency, while a narrow low energy IEDF can meet the requirements of some plasma processes in very high frequency driven CCP sources. Using TVWs can also help to solve the problem of surface charging in dielectric etch trenches in high-aspect-ratio (HAR) plasma etch process [44, 45]. In these studies the electron velocity and angular distribution at the electrodes was controlled by tailoring the driving voltage waveform to adjust the duration of the sheath collapse at the wafer. For a short sheath collapse time and in order to balance the ion flux to this electrode, a reversed electric field is generated to accelerate electrons towards the wafer. As a consequence of this, higher electron velocities perpendicular to the wafer can be realized. In electronegative gas discharges, more different ion energies and ion fluxes at the two electrodes can be generated by TVWs as compared to electropositive argon discharges, which may be beneficial for plasma etching applications [46]. Using TVWs synthesized from consecutive harmonics of a low driving frequency of the order of 100 kHz allows to control the shape of the IEDF at the wafer by customizing the sheath electric field and allowing the ions to react to changes of this field [47–50]. In this way narrow peaks of the IEDF can be generated and moved along the energy axis, which is highly beneficial for etch selectivity and atomic layer precision [49].

In the present work we investigate the application of TVWs to control the generation of F atoms and its energy cost / energy efficiency separately from the ion energy at the electrodes in low pressure capacitively coupled CF$_4$ plasmas. On purpose, a simpler gas and plasma chemistry is selected as compared to gas mixtures used in commercial applications, since such scenarios can hardly be described realistically by simulations. Moreover, a multitude of effects acts in parallel making it more difficult to isolate and understand single phenomena in depth. In this work, we show how using VWT allows to tailor the electron energy distribution function (EEDF) to enhance the volume production of F atoms and its energy efficiency. This phenomenon is expected to be present in other, more complicated gas mixtures, too.

This paper is structured in the following way: in section 2, the PIC/MCC code used for the numerical studies is described and the stationary diffusion model for the calculation of the F atom density is introduced. The results are presented in section 3. This section is divided into two parts: The sources of the generation of F atoms and the axial profiles of the F atom density for the different driving voltage waveforms are discussed in the first part. In the second part, the reason for the more energy efficient generation rate of F atoms based on TVWs rather than classical single frequency operation is analyzed. Finally, conclusions are drawn in section 4.

2. Simulation methods

2.1. PIC/MCC model

A one-dimensional in space and three-dimensional in velocity space (1d3v) particle in cell simulation complemented with a Monte Carlo treatment of collision processes (PIC/MCC) in CF$_4$ is employed in this work. The particles traced in the simulations are electrons, CF$_3^+$, CF$_2^+$, CF$_3^-$ and F$^-$ ions, which are the dominant charged particle species and represent a subset of all species that exist in CF$_4$ plasmas [51, 52]. The list of collision processes of electrons with neutral gas molecules considered in the model (which is the same as in previous works [52, 53]) is shown in table 1. The number of reactive collision processes of CF$_3^+$, CF$_2^+$, CF$_3^-$ and F$^-$ ions with CF$_4$ molecules is 41, 26, 67 and 19, same as in [54]. These collision processes are simulated by using the ion-molecule collision model for endothermic reactions [51, 55, 56]. This large number of ion-CF$_4$ processes is classified according to their products in the simulation, and the details can be found in our previous work [57]. In addition to the reactive collisions, isotropic and anisotropic elastic collisions are also taken into account in the model. Note that in all reactions, including e-CF$_4$ and ion-CF$_4$ collisions, when the products of any collision are species that are not considered in the model, the new particles are not added, only the energy loss of the colliding charged particle is accounted for. In order to maintain charge conservation, the original (projectile) charged particles are retained after changing their energy and velocity. The list of recombination processes is shown in table 2 along with their rate coefficients. The data are taken from [58] for electron-ion recombination and from [59] for ion-ion recombination. These processes are treated in the simulation as outlined in [59, 60].

In this work, simulations are performed at a fixed pressure of 4 Pa and electrode gap of $L = 2.5$ cm. The temperature of the neutral gas is kept at 300 K, which is justified by the low pressure [61]. Such discharge conditions are similar to those typically used for plasma etching. At the electrode surfaces, we assume that 70% [61] of the electrons are reflected back into the plasma elastically, and the ion induced secondary electron emission coefficient is set to 0.01 based on the findings of [57].

Three types of driving voltage waveforms are used in this work as shown in figure 1:

1. Single frequency waveform:

$$\phi\left(t\right) = \phi_1 \cos\left(2\pi f t\right) \qquad (1)$$

with low ($f = 13.56$ MHz) and high ($f = 67.8$ MHz) frequency, for which the voltage amplitude (ϕ_1) varies between 100 and 1000 V.

Table 1. Electron-CF$_4$ collisions considered in the model.

	Type of collision	Reaction	Threshold (eV)
1	Elastic momentum transfer	$CF_4 + e \rightarrow CF_4 + e$	0
2	Vibrational excitation	$CF_4 + e \rightarrow CF_4(v1) + e$	0.108
3	Vibrational excitation	$CF_4 + e \rightarrow CF_4(v3) + e$	0.168
4	Vibrational excitation	$CF_4 + e \rightarrow CF_4(v4) + e$	0.077
5	Electronic excitation	$CF_4 + e \rightarrow CF_4^* + e$	7.54
6	Dissociative ionization	$CF_4 + e \rightarrow CF_3^+ + F + 2e$	16
7	Dissociative ionization	$CF_4 + e \rightarrow CF_2^+ + 2F + 2e$	21
8	Dissociative ionization	$CF_4 + e \rightarrow CF^+ + 3F + 2e$	26
9	Dissociative ionization	$CF_4 + e \rightarrow C^+ + 4F + 2e$	34
10	Dissociative ionization	$CF_4 + e \rightarrow F^+ + CF_3 + 2e$	34
11	Dissociative ionization	$CF_4 + e \rightarrow CF_3^{2+} + F + 3e$	41
12	Dissociative ionization	$CF_4 + e \rightarrow CF_2^{2+} + 2F + 3e$	42
13	Attachment	$CF_4 + e \rightarrow F^- + CF_3$	5
14	Attachment	$CF_4 + e \rightarrow CF_3^- + F$	5
15	Neutral dissociation	$CF_4 + e \rightarrow CF_3 + F + e$	12
16	Neutral dissociation	$CF_4 + e \rightarrow CF_2 + 2F + e$	17
17	Neutral dissociation	$CF_4 + e \rightarrow CF + 3F + e$	18

Table 2. Recombination processes considered in the simulation.

Reaction	Rate coefficient (m^{3}s^{-1})
$CF_3^+ + e^-$	$3.95 \times 10^{-15} T_i^{-1} T_e^{-0.5}$
$CF_3^+ + F^-$	1×10^{-13}
$CF_3^+ + CF_3^-$	1×10^{-13}
$CF_2^+ + e^-$	$3.95 \times 10^{-15} T_i^{-1} T_e^{-0.5}$
$CF_2^+ + F^-$	1×10^{-13}
$CF_2^+ + CF_3^-$	1×10^{-13}

2. Peak-type waveforms given by:

$$\phi(t) = \sum_{k=1}^{N} \phi_k \cos(2\pi k f t) \qquad (2)$$

with the fundamental frequency of 13.56 MHz, with voltage amplitudes of the harmonics:

$$\phi_k = \frac{2(N-k+1)}{(N+1)^2} V_{pp}. \qquad (3)$$

The number of harmonics, N, is changed between 1 and 10, at a fixed value of the peak-to-peak voltage, V_{pp}, of 600 V.

3. Sawtooth up-type waveforms given by

$$\phi(t) = \phi_a \sum_{k=1}^{N} \frac{1}{k} \sin(2\pi k f t) \qquad (4)$$

with the fundamental frequency of 13.56 MHz. The integer value N is varied from 1 to 10. The voltage amplitude (ϕ_a) is set to ensure a peak-to-peak value of 600 V.

An external circuit is not included in the simulation. The dc self-bias in the peak-type and sawtooth up-type voltage waveform cases is determined in an iterative way to make sure that
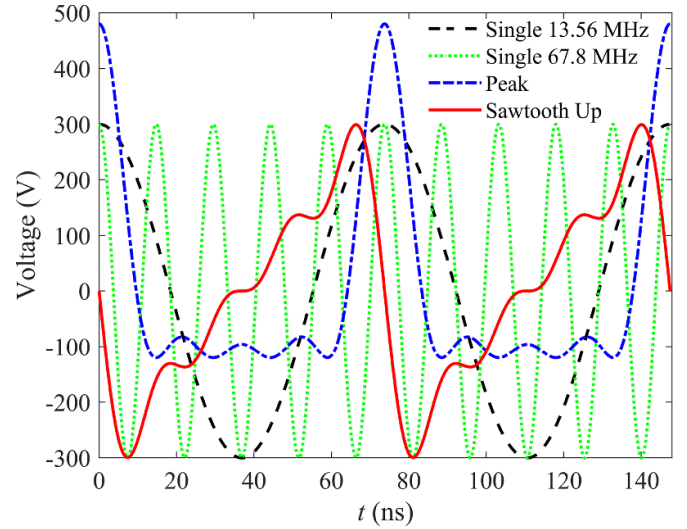
Figure 1. Driving voltage waveforms within two periods of the fundamental frequency (13.56 MHz).

the net charged particle flux to each of the electrodes per fundamental RF period becomes zero [62]. This PIC/MCC simulation of CCPs operated in CF$_4$ has been validated experimentally in the past [57, 63].

2.2. Stationary diffusion model to determine the F atom density profile

Based on previous studies of the F atom density in experiments [18, 20] and of fluorocarbon plasmas in simulation [64–66], we assume that F atoms are primarily formed in the volume by electron-neutral collisions under the conditions studied here and include these processes in our simulations. Adopting this assumption, the axial density profile of the F atoms, $n_F(x)$, can be obtained by solving the stationary diffusion equation
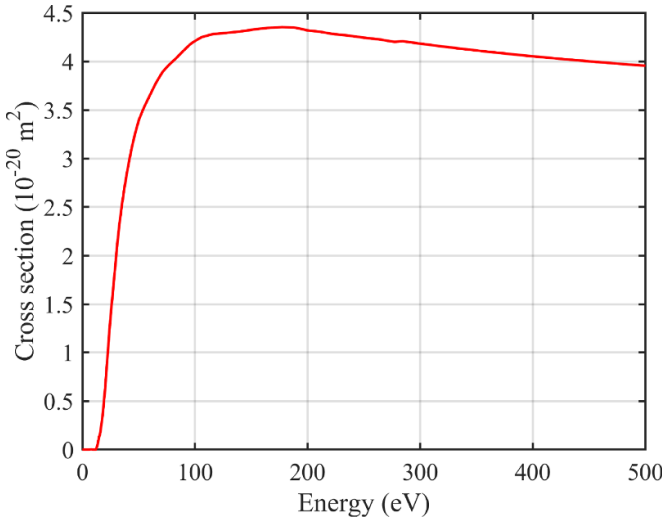
Figure 2. Total cross section of reactions that can produce F atoms in the simulation.

based on the space resolved and time averaged source function, $S_F(x)$, obtained from the PIC/MCC simulation:

$$-D\frac{\partial^2 n_F(x)}{\partial x^2} = S_F(x), \tag{5}$$

where D is the diffusion coefficient of F atoms in CF$_4$ gas calculated based on the Chapman–Enskog theory [67]:

$$D = \frac{1.86 \times 10^{-3} T^{3/2} \left(1/M_F + 1/M_{CF_4}\right)^{1/2}}{(p/101325)\,\sigma_{12}^2 \Omega}. \tag{6}$$

Here, T is the gas temperature in Kelvin ($T = 300$ K), p is the pressure in Pascal, and M_F and M_{CF_4} are the molecular weights of F and CF$_4$. The collision diameter $\sigma_{12} = (\sigma_F + \sigma_{CF_4})/2$ is the arithmetic average of the Lennard-Jones collision cross section of the F atoms ($\sigma_F = 2.968$ Å) and CF$_4$ molecules ($\sigma_{CF_4} = 4.662$ Å) [68]. The dimensionless quantity, Ω, is determined by the depths of the Lennard-Jones potential wells of F and CF$_4$ ($\varepsilon_F = 112.6$ K, $\varepsilon_{CF_4} = 134$ K) [68]. With these, equation (6) yields $D = 0.2135$ m^{2}s^{-1} for the diffusion coefficient, for the conditions studied.

The source function of F atoms, $S_F(x)$, includes F atom generation by electron impact dissociative ionization and neutral dissociation of CF$_4$ according to the processes listed in table 1, in the PIC/MCC simulation. The total cross section of electron impact reactions that produce F atoms in the model is given in figure 2. Potential surface production of F atoms, e.g. via fragmentation of incident CF$_3^+$ ions, is neglected [69], because the contributions of such wall production of F atoms to their density in the volume is not known well. While this clearly represents a simplification, we expect the proposed advantages of VWT to be functional even if such wall processes play an important role, since VWT enhances the production of ions in the volume, which will result in enhanced F atom production at the surface. Instead we include an effective loss coefficient (including reaction and recombination probabilities) of

F atoms at stainless steel surfaces of $\alpha_{loss} = 0.02$ [70]. The following boundary condition of the third kind is used for solving the diffusion equation for $n_F(x)$:

$$\frac{n_F(x=0/L)}{\kappa} = \left|\frac{\partial n_F}{\partial x}\right|_{x=0/L}, \tag{7}$$

where $\kappa = l(2 - \alpha_{loss})/(\sqrt{3}\alpha_{loss})$. l is the collisional mean free path of F atoms in CF$_4$ gas, which is calculated from the diffusion coefficient using [71]:

$$l = \frac{4}{\sqrt{3}\pi}\left(\frac{m}{3k_B T_g}\right)^{1/2} D. \tag{8}$$

Based on the diffusion coefficient and this boundary condition, equation (5) can be solved to obtain the time-averaged axial F atom density distribution, which is relevant for a variety of plasma processes [11, 72]. Note that F atoms are not considered as part of the background gas in the simulation in this work because of the low F atom density compared to the CF$_4$ density. However, under other discharge conditions, e.g. at high pressure, such neutral particles should be included via a hybrid model. Furthermore, our simulations predict the global energy cost of producing an F atom by electron impact dissociation, the physico-chemical model used to account for the production and losses of F atoms is simplified. Depending on the discharge conditions, the F atom production mechanisms may include fragmentation of CF$_x^+$ ions at surfaces, F atom loss processes may not obey a simple constant surface loss probability, and the recombination of CF$_x$ radicals in the volume might play a role. As a result, some deviations between measured F atom densities and the predictions of our simulations might occur. A careful experimental validation of these simulation results should, therefore, be performed in the future.

3. Results

This section is divided into two parts. In the first part, the sources of the F atom generation and the axial distribution of the F atom density calculated according to the stationary diffusion model for the various types of excitation waveforms are presented and discussed. In the second part, the energy cost / energy efficiency of the generation of F atoms and the option to control the F atom density separately from the ion energy at the electrodes are compared and analyzed for different types of driving voltage waveform shapes.

3.1. Generation and density profiles of F atoms

We present results for CCPs generated by low (13.56 MHz) and high (67.8 MHz) single frequency sinusoidal driving voltage waveforms, as well as for peak- and sawtooth-up TVWs synthesized from different numbers of consecutive harmonics of 13.56 MHz. For the cases of sinusoidal waveforms, the voltage amplitude is the control parameter for the F atom density and is varied in the range of 100–1000 V, while for the
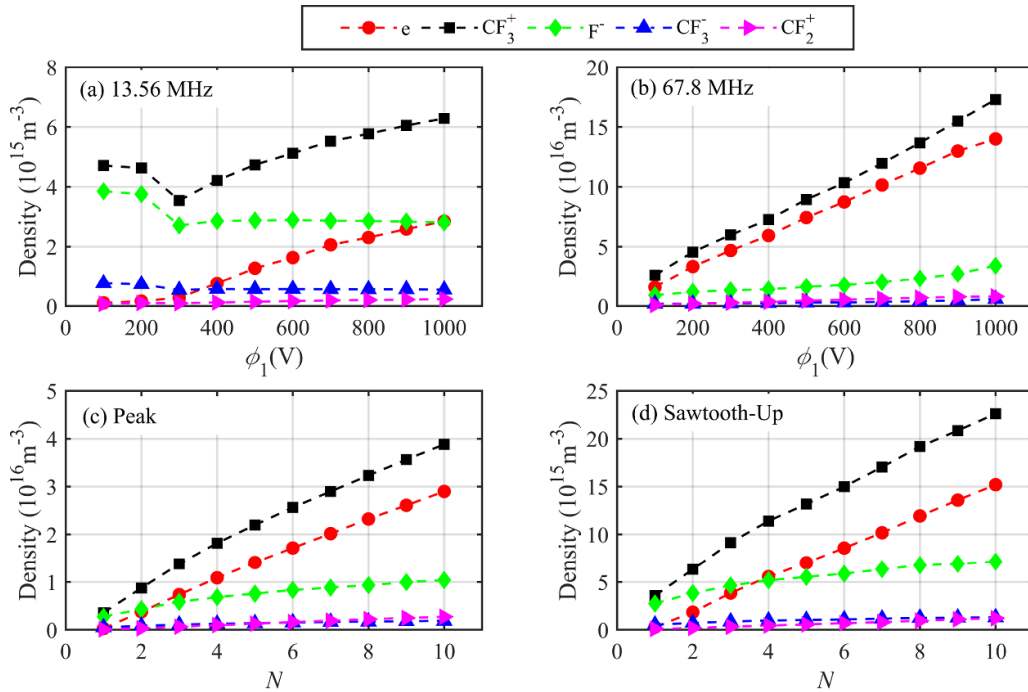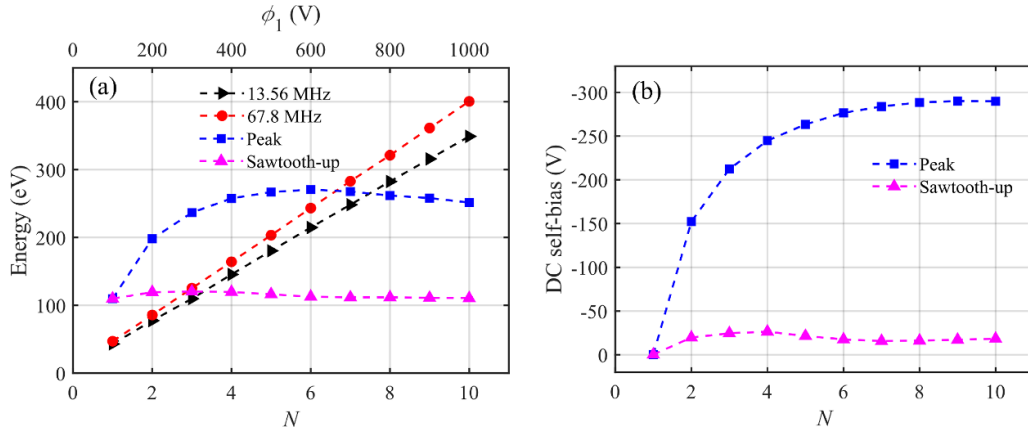
Figure 3. Spatially and temporally averaged densities of various charged species as a function of the driving voltage amplitude at 13.56 MHz (a), 67.8 MHz (b) and of the number of consecutive harmonics used to synthesize the peak (c), and sawtooth-up waveform (d) cases.

TVWs the number of consecutive harmonics of 13.56 MHz is the control parameter and is varied from 1 to 10 with a fixed peak-to-peak voltage of 600 V. The other discharge conditions are 2.5 cm electrode gap and 4 Pa pressure.

The plasma density and electronegativity are fundamental parameters of industrial interest. Figure 3 shows the spatially and temporally averaged charged particle densities as a function of the driving voltage amplitude for discharges driven by single frequency sinusoidal waveforms in (a) and (b), and as a function of the number of consecutive harmonics used to synthesize the TVWs in (c) and (d). In the case of 13.56 MHz excitation, within the range of voltage amplitudes between 100 and 1000 V, CF_3^+ and F^- ions are the dominant charged particles. The electron density increases with increasing voltage, but remains below the F^- ion density, resulting in a discharge of electronegative nature. These ion densities decrease first when the voltage increases from 100 V to 300 V, because the discharge is operated in the drift-ambipolar (DA) mode [73], characterized by a low electron density and high electric field in the plasma bulk. Increasing the driving voltage amplitude within this range results in an increase of the electron density. This induces a mode transition from the DA- to the α-mode, that results in an attenuation of the bulk electric field and in a decrease of the electron energy. This, in turn reduces the rates of ion generation and, thus, the ion densities decrease. Once the driving voltage amplitude is higher than 300 V, the CF_3^+ and electron density increase, while the densities of the other types of ions remain nearly constant as a function of the voltage. The heating of electrons mainly originates from the interaction with the expanding sheath, as will be shown later in figure 11.

In single frequency plasmas operated at 67.8 MHz (see figure 3(b)), electrons are always the dominant negatively charged species and the discharge is electropositive. The densities of all species increase as a function of the driving voltage amplitude. For the cases of peak- and sawtooth-up voltage waveforms (see figures 3(c) and (d)), when the number of consecutive harmonics is small, e.g. $N = 2$ for the peak-waveform and 4 for the sawtooth-up voltage waveform, the F^- ion density is higher than the electron density. For high numbers of consecutive harmonics, the electron density increases faster than the negative ion densities, exceeding all negative ion densities. The rapid increase of the electron density for the TVW cases is related to the dynamics of the electron power absorption, which will be analyzed in the next section.

Figure 4 shows the mean energy of CF_3^+ ions at the powered electrode as a function of the driving voltage amplitude (single frequency cases) and the number of harmonics at constant peak-to-peak voltage of 600 V (TVWs) as well as the DC self bias as a function of the number of harmonics (TVWs). For the single frequency cases the DC self-bias is zero independently of the driving voltage amplitude due to the geometrical and electrical symmetry of the discharge. Increasing the driving voltage amplitude in the single frequency cases leads to an increase of the mean ion energy, since the sheath voltages are increased. For peak TVWs, increasing N enhances the amplitude asymmetry of the driving voltage waveform so that the absolute value of the DC self bias and the ion bombardment energy at the powered electrode increase, while the ion energy at the grounded electrode decreases (not shown). For sawtooth-up TVWs, the DC self bias remains approximately constant as a function of the number of harmonics used to

Figure 4. Mean CF_3^+ ion energy at the powered electrode as a function of the driving voltage amplitude (single frequency cases) and the number of harmonics at constant peak-to-peak voltage (TVWs) (a) and DC self bias as a function of the number of harmonics at constant peak-to-peak voltage of 600 V (TVWs) (b).
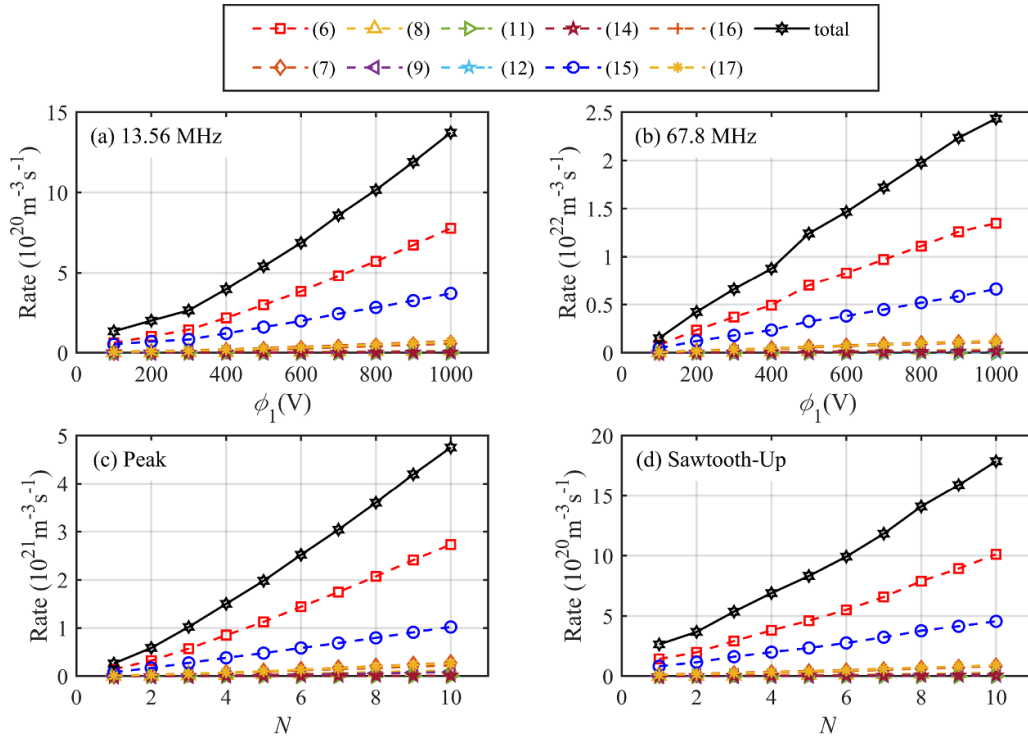

Figure 5. Spatially and temporally averaged F atom generation rate as a function of the driving voltage amplitude at 13.56 MHz (a), 67.8 MHz (b) and of the number of consecutive harmonics used to synthesize the peak-type (c), and sawtooth-up waveforms (d). The numbers in the legend refer to the respective process in table 1.

synthesize the driving voltage waveform, because there is no amplitude asymmetry for this waveform shape. Increasing N changes the slope asymmetry, which leads to a faster sheath expansion at the powered and a slower sheath expansion at the grounded electrode. However, due to the low pressure and the non-local electron dynamics this does not have a strong effect on the plasma symmetry and, thus, only small values of DC self-bias are observed, which are caused by the slope asymmetry of the driving sawtooth waveform.

There are various processes through which F atoms can be generated in CF_4 plasmas. From the list of electron-neutral

collisions considered in the model and listed in table 1, dissociative ionization and neutral dissociation are the primary processes. The spatially and temporally averaged reaction rates of each reaction with the product of an F atom are shown in figure 5. For the single frequency cases in figures 5(a) and (b), all the reaction rates increase as a function of the driving voltage amplitude, and in TVW driven plasmas, all the reaction rates increase as a function of the number of consecutive harmonics at a fixed peak-to-peak voltage of 600 V. Note that dissociative ionization, process (6), resulting CF_3^+ as a product is the most important reaction to produce F atoms, followed by
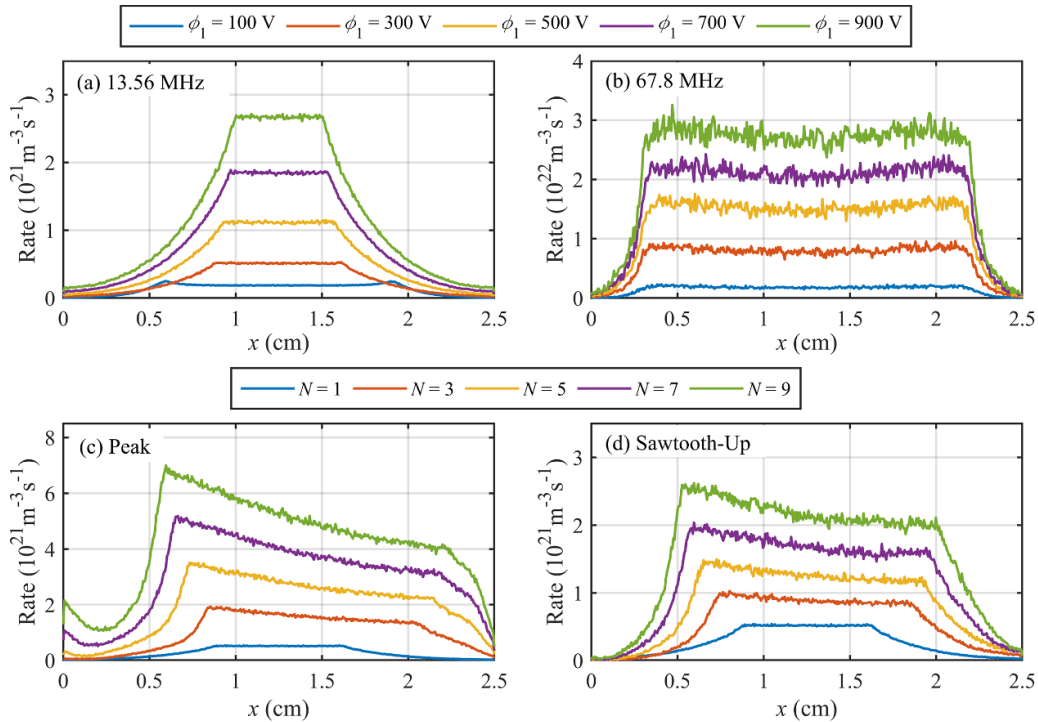
Figure 6. Time averaged total F atom generation rate profiles at different driving voltage amplitudes at 13.56 MHz (a), 67.8 MHz (b) and for different numbers of consecutive harmonic used to synthesize the peak-type (c), and the sawtooth-up driving voltage waveforms (d).

neutral dissociation, process (15), because of their large cross sections.

The spatial distributions of the various F atom generation rates for the different types of driving voltage waveforms are shown in figure 6. The total generation rate of F atoms is obtained by summing up all the individual reaction rates that produce F atoms. For reactions that produce more than one F atom, the reaction rate is multiplied by the number of the generated F atoms. In figures 6(a) and (b), the spatial profile of the F atom generation rate is symmetric for the sinusoidal driving voltage cases. For the 13.56 MHz case, when the driving voltage amplitude equals 100 V, the maxima of the F atom generation rate are located at the sheath edges because of the high ionization rate caused by the energetic electrons accelerated by the local ambipolar electric field. With the increase of the driving voltage amplitude, the F atom generation rate is enhanced, but the plasma bulk region is compressed, resulting in a narrow F atom generation rate profile and a 'volcanic-cone'-like shape. At a driving frequency of 67.8 MHz, the F atom generation rate almost fills the entire space between the electrodes because of the compressed sheath regions caused by the high plasma density. The rate also increases as a function of the driving voltage amplitude. For the TVW cases shown in figures 6(c) and (d), the F atom generation rate becomes asymmetric at higher numbers of consecutive harmonics used to synthesize the TVW, i.e. the generation of F atoms is stronger near the powered electrode compared to the grounded electrode. This asymmetry is stronger for the peak-type compared to the sawtooth-up case, since the DC self-bias in the peak-type voltage waveform driven plasma is higher than that in the

case of the sawtooth waveform as shown in figure 4(b). The increase of the F atom generation rate towards the powered electrode ($x = 0$), shown in figure 6(c), is caused by energetic electrons accelerated towards this electrode by a reversed electric field during the local sheath collapse, which will be discussed in more detail later in figure 12.

Based on the stationary diffusion model, the F atom generation rate shown in figure 6 can be used as input parameter to determine the axial F atom density profile. Figure 7 shows the axial distribution of the F atom density for the three different driving voltage waveforms. The F atom density is in the same order of magnitude as that obtained experimentally at similar discharge condition in [21], which verifies the accuracy of our computational results. For the sinusoidal driving voltage waveform cases, the F atom density increases with the voltage amplitude and its distribution exhibits a more pronounced central peak at 13.56 MHz compared to the 67.8 MHz case due to the volcanic-cone-like shape of the F atom generation rate in the former case. In figures 7(c) and (d), the F atom density increases with the number of harmonics, while the peak-to-peak driving voltage remains constant. Similar to the axial profile of the F atom generation rate, there is also an axial asymmetry of the F atom density profile, i.e. the densities are slightly different at both electrodes. However, this asymmetry of the F atom density is small and can hardly be noticed due to the relatively weak asymmetry of the profile of the F atom generation rate and the large distance of its maximum from the adjacent electrode at the low pressure used in this work. A higher F atom density develops in the peak-type driving voltage waveform case attributed to the higher
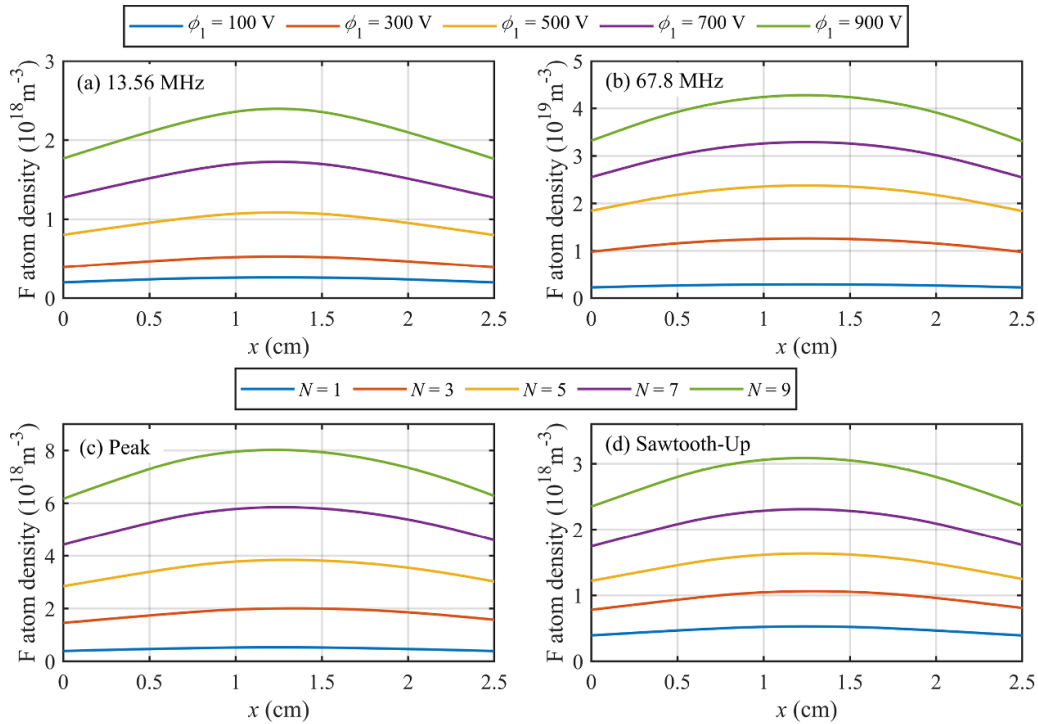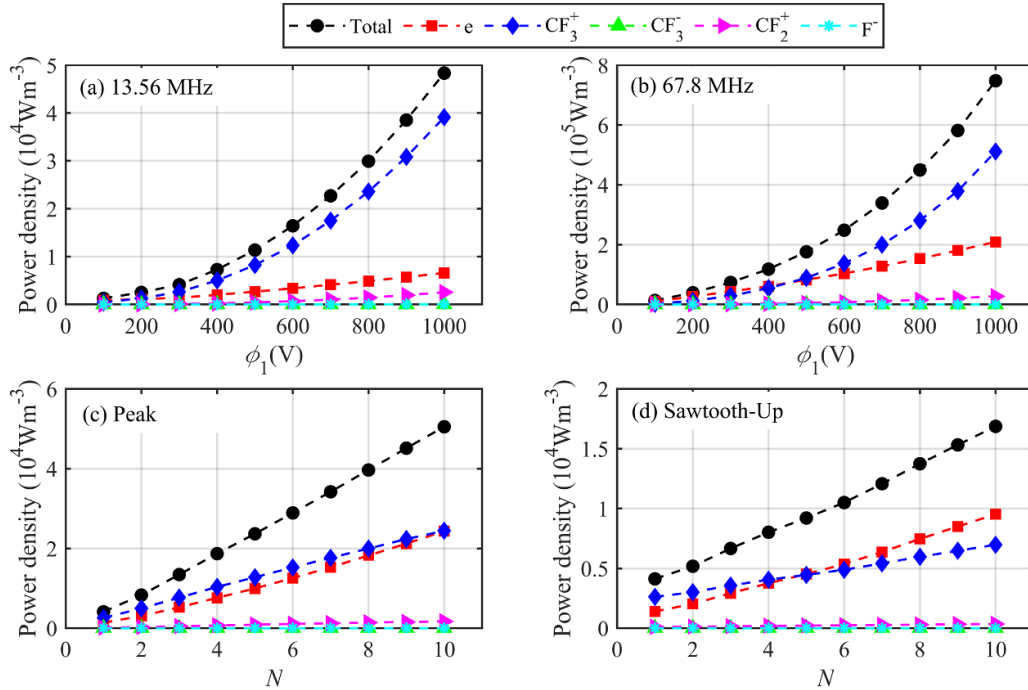
Figure 7. Time averaged axial F atom density distributions at different driving voltage amplitudes at 13.56 MHz (a), 67.8 MHz (b) and for different numbers of consecutive harmonics used to synthesize the peak-type (c), and the sawtooth-up driving voltage waveform (d) at constant peak-to-peak voltage.

F atom generation rate near the sheath region caused by the faster sheath expansion and the reversal of the electric field during the sheath collapse, which will be discussed in more detail later (see figure 12). In these four cases, the density of F atoms is highest in the 67.8 MHz single frequency case, followed by the peak waveform case. However, for applications the pursuit of a high F atom density to enhance the etch rate is one aspect, but the issue of energy efficiency for the generation of this radical is another important aspect. Moreover, the F atom density should ideally be controlled separately from the ion energy and high driving voltages at high frequencies should be avoided to prevent electromagnetic effects, that can induce non-uniformities. Therefore in the next subsection, the energy cost / energy efficiency of F atom generation and its separate control from the ion energy will be discussed.

3.2. Effects of the driving voltage waveform shape on the energy cost / efficiency of F atom generation and its separate control from the ion energy

Figure 8 shows the space and time averaged power absorbed by each charged particle species separately and the total absorbed power as a function of the driving voltage amplitude for the single frequency cases in (a, b), and as a function of the number of consecutive harmonics at fixed peak-to-peak voltage of 600 V for the TVWs in (c) and (d). For each species the absorbed power (P_j) is obtained based on their current density (J_j) and the electric field E as $P_j = J_j \cdot E$, where j indicates the type of species. With the increase of the driving voltage amplitude or the number of consecutive harmonics, the absorbed

power of all charged species is enhanced. For the single frequency cases, the total absorbed power increases faster at higher voltage amplitudes, which is mainly due to the power absorption by positive CF_3^+ ions in the sheaths. However, most of the energy absorbed by these ions is lost at the electrodes, when the ions hit the boundary surfaces, and is not used for the generation of F atoms. As shown in figure 8(b), an increase of the voltage amplitude at the high frequency of 67.8 MHz can more significantly increase the electron power absorption through the interaction of electrons with the rapidly expanding sheaths compared to that in the lower frequency scenario. This leads to a high ionization rate during the sheath expansion as shown in figure 11 and explains why the electron and F atom densities are the highest in this case. At the same time, the power absorbed by the ions also increases significantly. Thus, increasing the electron and F atom density by increasing the driving voltage amplitude in single frequency CCPs comes at the cost of dissipating a high fraction of the total dissipated power to the ions rather than the electrons. According to figures 4 and 7 tuning the driving voltage amplitude does not allow to separately control the F atom density and the mean ion energy at the electrodes. This high power absorbed by the ions due to the high sheath voltages (caused by the high driving voltage amplitude) cannot be used to accelerate electrons to high enough energies to generate F atoms via high energy threshold electron-neutral collisions. For some applications, e.g. reactive ion etching or high aspect ratio etching, the presence of highly energetic ions is required in addition to the presence of high radical fluxes so that increasing the driving voltage amplitude to some extent is useful for this

Figure 8. Spatially and temporally averaged power absorption density of charged species at different driving voltage amplitudes at 13.56 MHz (a), 67.8 MHz (b) and for different numbers of consecutive harmonics at fixed peak-to-peak voltage for peak-type (c), and the sawtooth-up tailored voltage waveforms (d).

purpose. However, often the ion energy must be above a certain threshold value and increasing it further is not useful, while the radical fluxes should be enhanced as much as possible. Generally, separate control of the flux of energetic ions, their energy and of the flux of radicals to the wafer is desirable, but cannot be achieved by simply increasing the driving voltage amplitude.

For the TVWs, the situation is very different, since the control parameter is not the driving voltage amplitude, but the waveform shape, which is controlled by changing the number of consecutive harmonics (and the harmonics' phases). In this case, the power absorbed by all the charged particles increases as a function of the number of harmonics. In the case of the peak-type waveform, as shown in figure 8(c), a similar fraction of the total dissipated power is absorbed by the electrons and the CF_3^+ ions—in strong contrast to the single frequency scenarios. And for the case of the sawtooth-up waveform, as shown in figure 8(d), the power absorbed by electrons will even exceed that of CF_3^+ ions, if the number of harmonics is larger than 5. Based on figures 4 and 7 separate control of the F atom density and mean ion energy by tuning N is possible for the sawtooth waveform.

Based on the F atom generation rate, shown in figure 5, and the total absorbed power density, shown in figure 8, the energy required to generate a single F atom can be determined as the ratio of the power density to the F atom generation rate, ξ_F, representing the energy cost required to produce an F atom. The dependencies of ξ_F on the driving voltage amplitude (single frequency cases) and the number of harmonics (TVWs) are shown in figure 9(a). As the generation of

F atoms is mainly determined by collisions of electrons with the neutral gas, the energy cost of the generation of a single electron is also determined as ξ_e and shown in figure 9(b). Based on figure 9(a), the energy required for generating an F atom increases as a function of the driving voltage amplitude for the single frequency cases for both the low and high driving frequency, with the latter being somewhat more effective. This is mainly caused by the enhanced power dissipation to ions at higher driving voltage amplitudes due to the higher sheath voltages. However, for the TVW cases, the energy cost to produce an F atom decreases as a function of the number of consecutive harmonics. The dependence of ξ_e on the driving voltage amplitude and the number of harmonics is similar to that of ξ_F. As the fraction of the total energy absorbed by the electrons is highest in the sawtooth-up case (see figure 8(d)), the energy cost to produce an electron or an F atom is minimum for this driving voltage waveform shape, i.e. the energy efficiency for producing electrons and F atoms is highest. For the TVWs, the energy cost of F atom generation decreases as a function of the number of consecutive harmonics used to synthesize the TVW. We note that a low number of consecutive harmonics, N, is sufficient to realize a high energy efficiency. As the peak-to-peak driving voltage and the DC self bias remain essentially unchanged for the sawtooth waveforms, the ion energy is approximately constant as a function of the number of harmonics (see figure 4). Thus, the F atom flux to the electrodes can be controlled separately from the ion energy by adjusting the shape of this driving voltage waveform in contrast to the standard single frequency discharges.
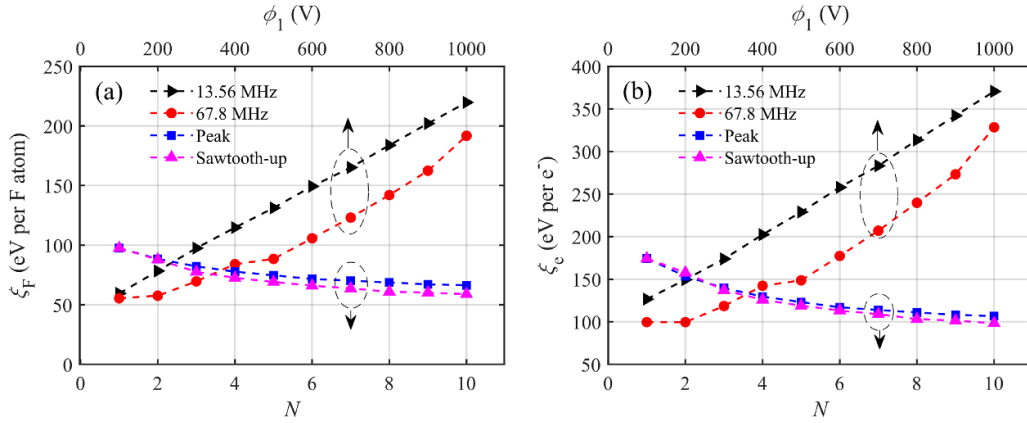
Figure 9. Energy cost to produce an F atom, ξ_F, (a) and an electron, ξ_e, (b) as a function of the driving voltage amplitude for the single frequency cases (upper scale) and as a function of the number of harmonics for the tailored voltage waveform cases (lower scale). The dashed ellipses and the arrows indicate the relevant control parameter (horizontal axes).
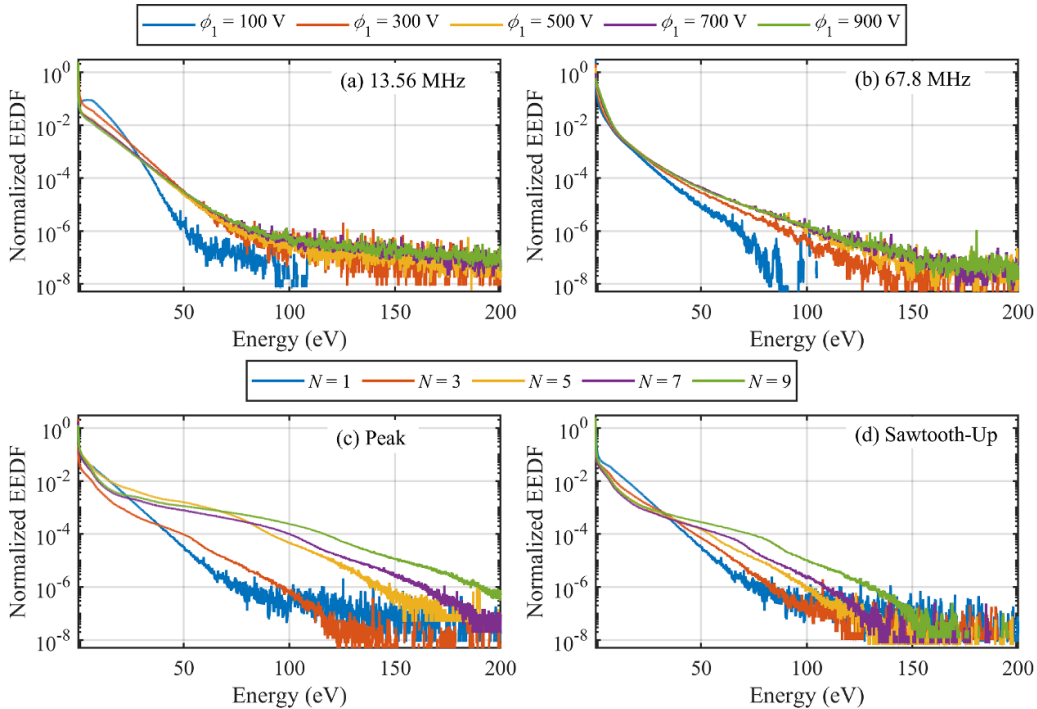

Figure 10. Normalized EEDFs at different driving voltage amplitudes for the single frequency cases at 13.56 MHz (a), 67.8 MHz (b) and for different numbers of consecutive harmonics used to synthesize the peak (c) and sawtooth-up (d) waveforms at fixed peak-to-peak voltage of 600 V. The EEDFs are obtained by spatio-temporally averaging the simulation results over the regions of interest indicated by the dashed rectangles in figures 11 and 12, respectively.

The reaction threshold electron energies related to the generation of F atoms are relatively high ($\geqslant 12\,\mathrm{eV}$) as shown in table 1. The effects of the driving voltage waveform shape on the energy cost of F atom generation can be understood based on the analysis of their effects on the EEDF, which is controlled by the spatio-temporal dynamics of energetic electrons [74]. Figure 10 shows the normalized EEDFs averaged over different spatio-temporal regions of interest (ROI), which are indicated by rectangles in the spatio-temporal plots of the ionization rate in figures 11 and 12. These regions contain the maximum of the ionization rate during sheath expansion, i.e. within these ROIs energetic electrons are present that

cause F atom production. And it is selected in a way that the region covers one quarter of the sheath expansion phase and one eighth of the distance between the electrodes. Note that in the sinusoidal cases, the size of the ROIs is, thus, the same in all cases, while in the TVW cases, the size of the ROIs is different because of the different duration of the sheath expansion phase. We can see that dissociative ionization is the dominant source of F atoms, i.e. the ionization rate reflects the F atom generation rate. Note that the EEDFs for $N = 1$ in the TVW cases correspond to the EEDF for the 13.56 MHz single frequency case at 300 V. As shown in figure 11, the ionization rate distributions are symmetric in space and time for the
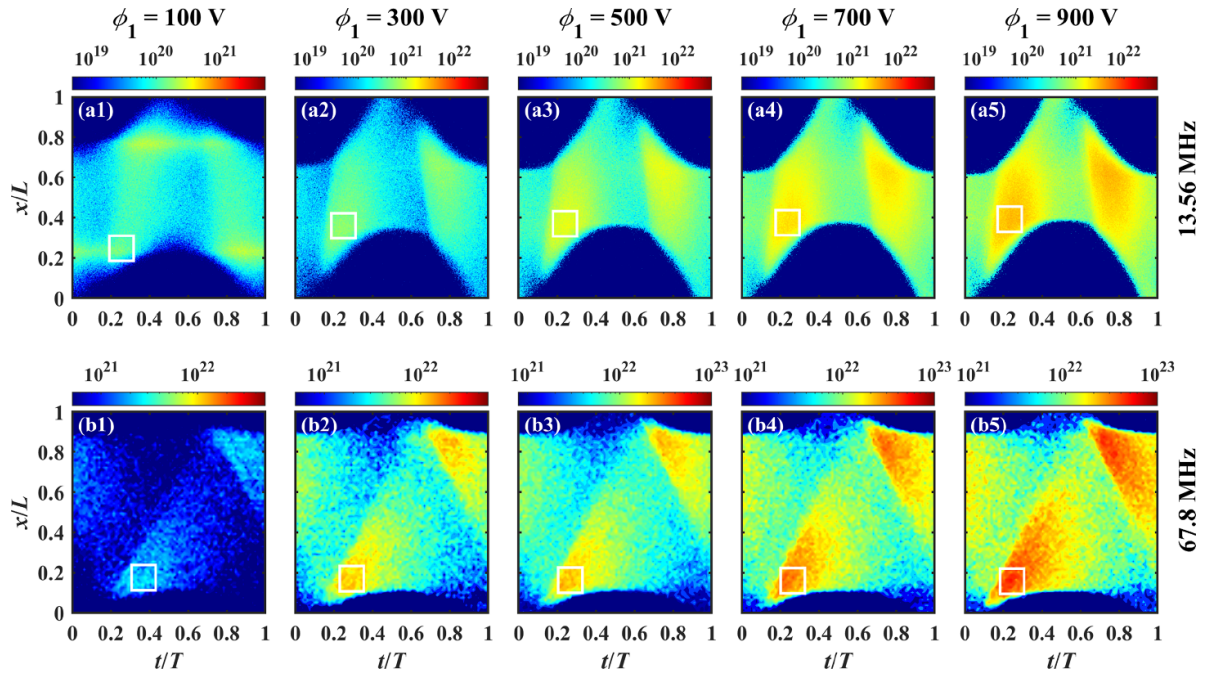
Figure 11. Spatio-temporal distributions of the ionization rate at different driving voltage amplitudes for single-frequency excitation at 13.56 MHz (first row) and 67.8 MHz (second row). The dashed rectangles indicate regions of interest over which the simulation data are averaged to obtain the EEDFs shown in figure 10. The units of the color scale are $m^{-3}s^{-1}$.
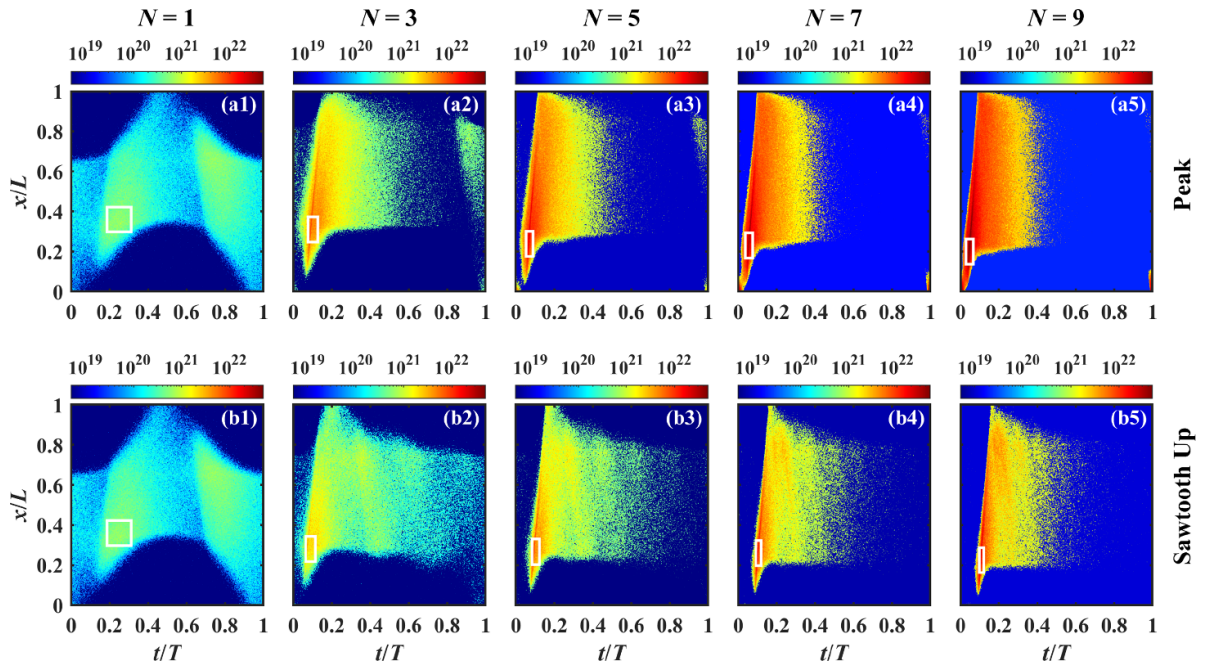
Figure 12. Spatio-temporal distributions of the ionization rate at different numbers of harmonics used to synthesize the peak- (first row) and the sawtooth-up driving voltage waveform (second row) at constant peak-to-peak voltage. The dashed rectangles indicate regions of interest over which the simulation data are averaged to obtain the EEDFs shown in figure 10. The white arrow in (a5) indicates an ionization maximum induced by a local electric field reversal. The units of the color scale are $m^{-3}s^{-1}$.

single frequency scenarios. For the 13.56 MHz case, at the low voltage of 100 V, the discharge is operated in the DA mode and the maximum ionization rate occurs at the edges of the collapsing sheaths because of the high local ambipolar electric field in this strongly electronegative plasma. Within the ROI used to extract the EEDF, which is located on the bulk side of

the sheath edge at the powered electrode during its expansion phase, there are only a few high-energy electrons for a driving voltage amplitude of 100 V, which leads to a weakly populated high energy tail of the EEDF as shown in figure 10(a), because the discharge is operated in the DA-mode. Above 300 V the discharge operation mode changes to a hybrid mode, which is

dominated by the α-mode with the ionization maximum located near the expanding sheath edges. A beam of energetic electrons is generated by ambipolar electron power absorption during sheath expansion that propagates into the plasma bulk due to the long electron mean free path at low pressure and the drift electric field in the bulk. Therefore, the high-energy tail of the EEDF is populated more strongly within the ROI used to analyze the data. After the discharge mode transition, with the increase of the driving voltage amplitude, the ionization rate is enhanced because of the increased electron density, but the electron power absorption dynamics does not change. Thus, as shown in figure 10(a), besides the change of the EEDF caused by the mode transition, i.e. the more enhanced high-energy tail when the voltage is higher than 300 V, the dependence of the EEDF shape on the voltage is limited. The fraction of high-energy electrons among all electrons does not increase as a function of the voltage, so that the energy cost of producing electrons and F atoms cannot be decreased in this way. In fact, with the increase of the driving voltage amplitude, more energy is dissipated to the ions causing the energy efficiency of F atom production to decrease. A similar scenario occurs in the case of 67.8 MHz. With the increase of the voltage, the maximum ionization rates at the expanding sheath edges are enhanced, but the electron power absorption dynamics is not changed, showing a marginal effect on the EEDF shape (see figure 10(b)).

The situation is different for TVWs, which allow to control the spatio-temporal distribution of the ionization rate efficiently at constant peak-to-peak voltage as shown in figure 12. The asymmetry of this ionization rate distribution is enhanced by increasing the number of harmonics, N, which changes the shape of the driving voltage waveform in a way that induces a faster expansion of the sheath near the powered electrode. For the peak waveform case, as shown in the first row of figure 12, if the number of driving harmonics is higher than 1, ionization will mainly occur in the first half of the RF period during the fast sheath expansion near the powered electrode. A weak ionization rate maximum can also be seen near the upper (grounded) electrode when the adjacent sheath expands. As the number of driving frequencies is increased, the spatio-temporal ionization maximum at the bottom electrode during sheath expansion gets stronger, since the driving voltage waveform induces a faster local sheath expansion. A weak local ionization maximum also appears in the lower right corner of the spatio-temporal distributions, when the sheath collapses in figures 12(a2)–(a5) caused by a local electric field reversal, of which one is indicated by a white arrow in (a5). Within the region of interest indicated by the dashed rectangle, when the sheath at the powered electrode expands, the use of a peak-waveform effectively enhances the power absorption of electrons, producing a higher number of energetic electrons that can generate new electrons via ionization and F atoms by ionization and dissociation. Ultimately, this leads to an enhancement of the high-energy tail of the EEDF especially at around 100 eV being at the position of high cross section of reactions that produce F atoms as shown in figure 2 in this ROI in

figure 10(c) and a significant enhancement of the energy efficiency of F atom and electron generation by controlling the EEDF shape by voltage waveform tailoring.

For the case of the sawtooth-up waveform, as shown in the second row of figure 12, a similar effect of increasing the number of driving frequencies is observed, i.e. the ionization maximum at the bottom powered electrode during sheath expansion is enhanced. Correspondingly, as shown in figure 10(d), the high-energy tail of the EEDF is enhanced at higher numbers of harmonics and the energy cost of F atom production is decreased. Compared to the peak-waveform case, an even lower energy cost is observed. This is caused by the fact that the high energy electrons generated by the fast sheath expansion near the powered electrode are confined better in the sawtooth-up as compared to the peaks-waveform case. As shown in figure 12 the beam of energetic electrons reaches the opposite grounded electrode during the local sheath collapse in case of the peaks-waveform, so that many energetic electrons are lost at this boundary surface. Due to the particular shape of the peaks-TVW, the sheath is collapsed for a long time within each fundamental RF period at the grounded electrode. This is different from the sawtooth case, for which the duration of the sheath collapse at this electrode is shorter so that some of the energetic beam electrons are reflected back into the bulk when the sheath expands immediately after the sheath collapse, i.e. less energetic electrons are lost to this electrode. This is a consequence of the different shape of the driving voltage waveform. In parallel the peak-to-peak voltage and the DC self bias remain constant so that the ion energy at the electrodes does not change much.

Overall, for applications a high density and flux of F atoms is typically desired, while ensuring an optimum energy efficiency of F atom generation. Based on figure 7, generating an F atom density of about 2.5×10^{18} m^{-3} requires a driving voltage amplitude of 900 V in a classical 13.56 MHz CCP and results in an energy cost of about 200 eV per F atom (see figure 9). The same F atom density can be realized based on a peak-waveform synthesized from 4 consecutive harmonics of 13.56 MHz with a much lower cost of only about 75 eV per F atom. High F atom densities can also be generated in single frequency discharges driven by higher frequencies at reasonable energy cost. However, as long as the control parameter for this radical density is the driving voltage amplitude or power, changing this control parameter will affect the ion energy and the energy efficiency of producing this radical drastically. Thus, better separate control is realized by using TVWs, especially sawtooth waveforms, where the peak-to-peak voltage can be kept constant. Moreover, using high voltage amplitudes in single high frequency CCPs can result in radial plasma non-uniformities due to electromagnetic effects. While still containing high frequency components, their amplitudes are lower for TVWs compared to single high frequency waveforms and such detrimental effects might be less pronounced. Generally, our results show that TVWs provide advanced control and flexibility for plasma processing applications.

4. Conclusions

RF discharges operated in low pressure fluorine-containing gases are widely used for the etching of SiO_2 in microelectronic circuit fabrication. In the etching process, atomic fluorine plays a crucial role in forming volatile products, such as SiF_4, thus etching the substrate. The F atom density is an important parameter which affects the etching rate.

In this work, we studied the main channels of F atom generation and the energy cost / energy efficiency of F atom generation in the presence of different driving voltage waveform shapes, i.e. sinusoidal waveforms with low (13.56 MHz) and high (67.8 MHz) frequency, peak and sawtooth-up TVWs, in capacitively coupled CF_4 plasmas by using a PIC/MCC simulation combined with a stationary diffusion model for the calculation of the F atom density profile. In both sinusoidal voltage waveform cases, the voltage was varied from 100 V to 1000 V, and in the TVW cases, the peak-to-peak voltage was fixed at 600 V and the number of the harmonics composing the waveform was changed from 1 to 10 to tailor the waveform shape. The other discharge conditions were kept constant at 4 Pa pressure and 2.5 cm electrode gap.

Our results demonstrate that in CF_4 plasmas electron impact ionization and neutral dissociation with the production of CF_3^+ ions and CF_3 molecules, respectively, are the main channels of F atom generation. In the cases of sinusoidal driving voltage waveforms, the rates of all the reactions that can produce F atoms and the F atom density exhibit a symmetrical axial distribution and are enhanced by increasing the voltage amplitude. The energy cost of F atom and electron generation was found to increase as a function of the driving voltage amplitude, since more energy is absorbed by the ions due to an increase of the sheath voltages. The EEDF shape cannot be controlled efficiently in this way and no separate control of the ion energy and the F radical flux can be realized.

However, TVWs were found to result in a lower energy cost of F atoms and electron production as well as in more advanced control options. Applying peaks- and sawtooth-up waveforms synthesized from different numbers of consecutive harmonics of 13.56 MHz was found to induce asymmetric ionization dynamics. The ionization rate during the fast sheath expansion phase near the powered electrode was enhanced as a function of the number of driving harmonics, since the shape of the driving voltage waveform induces a faster local sheath expansion. This increase in energy absorbed by electrons results in an enhancement of the high-energy tail of the EEDF in the region of maximum ionization. This was found to lead to an increase of the generation rate of electrons and F atoms and a better energy efficiency of their production at constant peak-to-peak voltage. For sawtooth-up waveforms, the mean ion energy at the electrodes remained constant so that separate control of the F atom density and the mean ion energy via Voltage Waveform Tailoring is possible. The lowest energy cost occurred in the sawtooth-up case because of the better confinement of high energy electrons compared to the peak case.

We demonstrated that TVWs can efficiently control the dynamics of energetic electrons and provide a lower energy cost of the F atom generation as compared to classical single frequency CCPs as well as separate control of the F atom density from the ion energy. We expect that the F atom density and flux generated with low energy cost by TVW driven plasmas and the advanced control options can improve the energy efficiency and control of plasma processes and serves as an example of knowledge-based plasma process development and improvement.

Data availability statement

The data that support the findings of this study are available upon reasonable request from the authors.

Acknowledgments

ORCID iDs

Xiao-Kun Wang ⬤ https://orcid.org/0000-0003-4160-5316
Ranna Masheyeva ⬤ https://orcid.org/0000-0002-6950-662X
Yong-Xin Liu ⬤ https://orcid.org/0000-0002-6506-7148
Yuan-Hong Song ⬤ https://orcid.org/0000-0001-5712-9241
Peter Hartmann ⬤ https://orcid.org/0000-0003-3572-1310
Zoltán Donkó ⬤ https://orcid.org/0000-0003-1369-6150
Julian Schulze ⬤ https://orcid.org/0000-0001-7929-5734

References

[1] Lieberman M A and Lichtenberg A J 2005 *Principles of Plasma Discharges and Materials Processing* (Wiley)
[2] Chabert P and Braithwaite N 2011 *Physics of Radio-Frequency Plasmas* (Cambridge University Press)
[3] Makabe T and Petrovic Z L 2006 *Plasma Electronics: Applications in Microelectronic Device Fabrication* (CRC Press)
[4] Kamisugi K T and Kawasaki T K T 1999 *Jpn. J. Appl. Phys.* **38** 4367
[5] Donnelly V M and Kornblit A 2013 *J. Vac. Sci. Technol.* A **31** 050825
[6] Kim M T 2000 *J. Electrochem. Soc.* **147** 1204
[7] Sasaki K, Kawai Y, Suzuki C and Kadota K 1998 *J. Appl. Phys.* **83** 7482–7
[8] Sasaki K, Kawai Y and Kadota K 1999 *Rev. Sci. Instrum.* **70** 76–81
[9] Economou D J 2000 *Thin Solid Films* **365** 348–67
[10] Takizawa K T K, Sasaki K S K and Kadota K K K 2001 *Jpn. J. Appl. Phys.* **40** 5130
[11] Flamm D L, Donnelly V M and Mucha J A 1981 *J. Appl. Phys.* **52** 3633–9
[12] Coburn J W and Chen M 1981 *J. Vac. Sci. Technol.* **18** 353–6

[13] Coburn J W and Chen M 1980 *J. Appl. Phys.* **51** 3134–6
[14] Booth J P and Sadeghi N 1991 *J. Appl. Phys.* **70** 611–20
[15] Kawai Y K Y, Sasaki K S K and Kadota K K K 1997 *Jpn. J. Appl. Phys.* **36** L1261
[16] Lopaev D V, Volynets A V, Zyryanov S M, Zotovich A I and Rakhimov A T 2017 *J. Phys. D: Appl. Phys.* **50** 075202
[17] Tachibana K and Kamisugi H 1999 *Appl. Phys. Lett.* **74** 2390–2
[18] Sasaki K, Kawai Y, Suzuki C and Kadota K 1997 *J. Appl. Phys.* **82** 5938–43
[19] Nakamura K N K, Segi K S K and Sugai H S H 1997 *Jpn. J. Appl. Phys.* **36** L439
[20] Tserepi A, Schwarzenbach W, Derouard J and Sadeghi N 1997 *J. Vac. Sci. Technol.* A **15** 3120–6
[21] Cunge G, Chabert P and Booth J P 2001 *J. Appl. Phys.* **89** 7750–5
[22] Goto H H, Löwe H and Ohmi T 1992 *J. Vac. Sci. Technol.* A **10** 3048–54
[23] Goto H, Lowe H D and Ohmi T 1993 *IEEE Trans. Semicond. Manuf.* **6** 58–64
[24] Gans T, Schulze J, O'Connell D, Czarnetzki U, Faulkner R, Ellingboe A R and Turner M M 2006 *Appl. Phys. Lett.* **89** 261502
[25] Bi Z-H, Dai Z-L, Zhang Y-R, Liu D-P and Wang Y-N 2013 *Plasma Sources Sci. Technol.* **22** 055007
[26] Schulze J, Gans T, O'Connell D, Czarnetzki U, Ellingboe A R and Turner M M 2007 *J. Phys. D: Appl. Phys.* **40** 7008–18
[27] Heil B G, Czarnetzki U, Brinkmann R P and Mussenbrock T 2008 *J. Phys. D: Appl. Phys.* **41** 165202
[28] Czarnetzki U, Heil B G, Schulze J, Donkó Z, Mussenbrock T and Brinkmann R P 2009 *J. Phys.: Conf. Ser.* **162** 012010
[29] Schulze J, Schüngel E and Czarnetzki U 2009 *J. Phys. D: Appl. Phys.* **42** 092005
[30] Schulze J, Schüngel E, Czarnetzki U, Gebhardt M, Brinkmann R P and Mussenbrock T 2011 *Appl. Phys. Lett.* **98** 031501
[31] Korolov I, Donkó Z, Czarnetzki U and Schulze J 2012 *J. Phys. D: Appl. Phys.* **45** 465205
[32] Schulze J, Derzsi A and Donkó Z 2011 *Plasma Sources Sci. Technol.* **20** 045008
[33] Lafleur T, Delattre P A, Johnson E V and Booth J P 2012 *Appl. Phys. Lett.* **101** 124104
[34] Lafleur T, Boswell R W and Booth J P 2012 *Appl. Phys. Lett.* **100** 194101
[35] Derzsi A, Horváth B, Donkó Z and Schulze J 2020 *Plasma Sources Sci. Technol.* **29** 074001
[36] Bruneau B, Novikova T, Lafleur T, Booth J P and Johnson E V 2014 *Plasma Sources Sci. Technol.* **23** 065010
[37] Bruneau B, Novikova T, Lafleur T, Booth J P and Johnson E V 2014 *Plasma Sources Sci. Technol.* **24** 015021
[38] Bruneau B, Gans T, O'Connell D, Greb A, Johnson E V and Booth J P 2015 *Phys. Rev. Lett.* **114** 125002
[39] Franek J, Brandt S, Berger B, Liese M, Barthel M, Schüngel E and Schulze J 2015 *Rev. Sci. Instrum.* **86** 053504
[40] Schmidt F, Schulze J, Johnson E, Booth J-P, Keil D, French D M, Trieschmann J and Mussenbrock T 2018 *Plasma Sources Sci. Technol.* **27** 095012
[41] Wang J, Dine S, Booth J P and Johnson E V 2019 *J. Vac. Sci. Technol.* A **37** 021303
[42] Sharma S, Sirse N and Turner M M 2023 *Phys. Plasmas* **30** 073506
[43] Sharma S, Sirse N, Kuley A and Turner M M 2021 *Phys. Plasmas* **28** 103502

[44] Krüger F, Wilczek S, Mussenbrock T and Schulze J 2019 *Plasma Sources Sci. Technol.* **28** 075017
[45] Hartmann P *et al* 2021 *J. Phys. D: Appl. Phys.* **54** 255202
[46] Bruneau B *et al* 2016 *J. Appl. Phys.* **119** 163301
[47] Buzzi F L, Ting Y H and Wendt A E 2009 *Plasma Sources Sci. Technol.* **18** 025009
[48] Qin X V, Ting Y H and Wendt A E 2010 *Plasma Sources Sci. Technol.* **19** 065014
[49] Faraz T, Verstappen Y G P, Verheijen M A, Chittock N J, Lopez J E, Heijdra E, van Gennip W J H, Kessels W M M and Mackus A J M 2020 *J. Appl. Phys.* **128** 213301
[50] Hartmann P, Korolov I, Escandón-López J, van Gennip W, Buskes K and Schulze J 2023 *J. Phys. D: Appl. Phys.* **56** 055202
[51] Georgieva V, Bogaerts A and Gijbels R 2003 *J. Appl. Phys.* **93** 2369–79
[52] Donkó Z and Petrović Z L 2006 *Jpn. J. Appl. Phys.* **45** 8151–6
[53] Schüngel E, Korolov I, Bruneau B, Derzsi A, Johnson E, O'Connell D, Gans T, Booth J P, Donkó Z and Schulze J 2016 *J. Phys. D: Appl. Phys.* **49** 265203
[54] Georgieva V 2006 Computer modeling of low-pressure fluorocarbon-based discharges for etching purposes *PhD Thesis* Universiteit Antwerpen, Belgium
[55] Nanbu K and Kitatani Y 1995 *J. Phys. D: Appl. Phys.* **28** 324
[56] Denpoh K and Nanbu K 1998 *J. Vac. Sci. Technol.* A **16** 1201–6
[57] Wang X K, Masheyeva R, Liu Y X, Hartmann P, Schulze J and Donkó Z 2023 *Plasma Sources Sci. Technol.* **32** 085009
[58] Rauf S and Kushner M J 1997 *J. Appl. Phys.* **82** 2805–13
[59] Denpoh K D K and Nanbu K N K 2000 *Jpn. J. Appl. Phys.* **39** 2804
[60] Nanbu K and Denpoh K 1998 *J. Phys. Soc. Japan* **67** 1288–90
[61] Schulenberg D A, Korolov I, Donkó Z, Derzsi A and Schulze J 2021 *Plasma Sources Sci. Technol.* **30** 105003
[62] Donkó Z, Schulze J, Heil B G and Czarnetzki U 2008 *J. Phys. D: Appl. Phys.* **42** 025205
[63] Liu Y X, Donkó Z, Korolov I, Schüngel E, Wang Y N and Schulze J 2019 *Plasma Sources Sci. Technol.* **28** 075005
[64] Toneli D A, Pessoa R S, Roberto M and Gudmundsson J T 2019 *Plasma Sources Sci. Technol.* **28** 025007
[65] Sankaran A and Kushner M J 2004 *J. Vac. Sci. Technol.* A **22** 1242–59
[66] Huang S, Huard C, Shim S, Nam S K, Song I C, Lu S and Kushner M J 2019 *J. Vac. Sci. Technol.* A **37** 031304
[67] Cussler E L 2009 *Diffusion: Mass Transfer in Fluid Systems* (Cambridge University Press)
[68] Hash D B, Bose D, Rao M V V S, Cruden B A, Meyyappan M and Sharma S P 2001 *J. Appl. Phys.* **90** 2148–57
[69] Booth J P, Cunge G, Chabert P and Sadeghi N 1999 *J. Appl. Phys.* **85** 3097–107
[70] Gudmundsson J T 2002 *J. Phys. D: Appl. Phys.* **35** 328
[71] Derzsi A, Hartmann P, Vass M, Horváth B, Gyulai M, Korolov I, Schulze J and Donkó Z 2022 *Plasma Sources Sci. Technol.* **31** 085009
[72] Williams P F 2013 *Plasma Processing of Semiconductors* vol 336 (Springer Science and Business Media)
[73] Schulze J, Derzsi A, Dittmann K, Hemke T, Meichsner J and Donkó Z 2011 *Phys. Rev. Lett.* **107** 275001
[74] Korolov I, Donkó Z, Hübner G, Bischoff L, Hartmann P, Gans T, Liu Y, Mussenbrock T and Schulze J 2019 *Plasma Sources Sci. Technol.* **28** 094001